'1'111': THERMALBALANCEOFTHEVENUSATMOSPHERE

DAVID CRISP
Jet Propulsion Laboratory, California Institute of Technology (add)
DMITRI TITOV
Space Research Institute, Moscow

Observations of the Venus thermal structure collected during the first three decades of the space age reveal high surface temperatures (730 K), near-adiabatic vertical temperature gradients throughout the lower atmosphere (0 58 km), and a reversed pole-to-equator mesospheric thermal structure, with polar temperatures that are ~ 20 K higher than those over the equator at altitudes between 70 and 100 km. The physical processes that maintain these anomalous features of the thermal balance were not completely understood when this topic was last reviewed in the early 1980's. Since that time, additional observations have provided an improved description of the atmospheric thermal structure and optical properties. Here, we summarize the new observational constraints provided by the *Venera 15*, *VEGA*, and *Galileo* missions, and those provided by Earth-based ultra-violet, near-infrared, and microwave observations. We also describe recent advances in modeling methods that have resolved some of the most perplexing issues, including *(i)* the need for unidentified thermal opacity sources to explain the high surface temperatures and atmospheric thermal flux distribution, *(ii)* the effects of reduced water vapor and cloud abundances on the greenhouse, and *(iii)* the processes that maintain the anomalously warm polar mesosphere.

1. 1N1'lWl)UC'J'loi%

Microwave observations collected during the 1950's provided the first evidence for the high surface temperatures and hot lower atmosphere of Venus [*Mayer et al* 1958; *Drake*, 1 962; *Kuz'min and Salomonovich*, should have radiative equilibrium brightness temperatures near 230 K, in remarkable agreement with values inferred from available infrared observations [*Moroz*, 1983]. The high microwave brightness temperatures therefore stimulated a spirited debate about their origin, and their implications for the Venus thermal balance.

Investigations of the thermal balance of the deep atmosphere of Venus were a major focus of both the US and Soviet space programs during the first two decades of the space age. *In-situ* measurements acquired by the *Venera 4-14* and *Pioneer Venus* (PV) entry probes confirmed that the atmospheric temperatures increase from ~225 K at the cloud tops (~65 km) to values near 730 K at the surface (Figure 1) [*Seiff*, 1983]. These observations also provided improved constraints on the composition and optical properties of the massive (90 bar), predominately CO_2 atmosphere. This information has been incorporated into progressively more sophisticated and reliable numerical radiative transfer models for studies of the thermal balance. These models indicate that the high surface temperatures are maintained by an efficient, solar-driven, atmospheric greenhouse mechanism [*Pollack, et al.* 1980], but there are several details of the deep-atmosphere thermal balance that are still poorly understood. In particular, observations and theoretical models available during the late 1970's and early 1980's indicated that the thermal opacity provided by known infrared-active gases (CO_2, H_2O, SO_2, HF, HCl) and H_2SO_4 aerosols might not be adequate to maintain temperatures as high as those observed at the surface and in the lower atmosphere of Venus. To produce the required thermal opacity, large numbers of tiny, invisible *Mode 1* particles were added to the clouds, almost doubling their total mass. The relatively stable temperature lapse rates observed throughout the deep atmosphere (Figure 2) are also poorly understood within the context of these greenhouse models, which require near-neutral stability (*i.e.* adiabatic lapse rates) at these levels. More recent observations, laboratory investigations, and modeling studies have provided improved constraints on the thermal opacity of the deep atmosphere, and contributed additional support for the greenhouse hypothesis. However, a complete, self-consistent model of the Venus deep atmosphere thermal structure has not yet been developed. The thermal balance of the deep atmosphere is reviewed in greater detail in Section IV.

Even though spacecraft and ground-based observations have provided new insight into the thermal balance of the deep atmosphere, they have also revealed a few additional surprises. Perhaps the most striking example is the discovery of the reversed equator-to-pole temperature gradients and the warm polar dipole structure at mesospheric levels [*Taylor et al.* 1979; 1980] (Figure 3). At altitudes between 70-90 km, the equator to pole temperature gradients reverse, such that polar regions are up to 20 K warmer than the equator *Taylor et al* 1979; 1980;

Kliore and Patel 1982; *Kliore* 1991]. The persistence of this anomalous thermal structure has been confirmed by routine *PV* and *Magellan* radio occultation observations, and by observations acquired in 1983 by the *Venera 15* spectrophotometer [*Zasova and Moroz* 1992] and those taken in 1990 by the *Galileo* Near Infrared Mapping Spectrometer (NIMS) [*Carlson et al.* 1991]. The radiative and dynamical processes responsible for maintaining this anomalous mesospheric temperature gradients were not yet known in the early 1980's when [*Taylor et al.* 1983] reviewed this topic in **Venus**. Modeling studies conducted during the 1980's have since provided a significant insight into these processes, however. These studies indicate that the observed thermal structure is a consequence of the interactions between the vertically-propagating atmospheric thermal tides and the zonal superrotation [*Fels and Lindzen* 1974; *Baker and Leovy* 1987; *Newman and Leovy*, 1992]. The thermal balance of the mesosphere is described in Section V.

II. THERMAL BALANCE METHODS

On a terrestrial planet, where internal sources contribute little to the

$$F_t = 4\pi r^2 \epsilon\sigma T_e^4 \qquad (2)$$

$$T_e = [(1 - a_s)F_{\odot} R_s^2/(4\epsilon\sigma R^2)]^{1/4} \qquad (3)$$

where $\sigma = 5.669 \times 10^{-8}$ W m^{-2} K^{-4} is the Stefan Boltzmann constant.

At a distance of 0.7233 AU from the sun, Venus receives almost twice as much solar radiation as the Earth (2624 *vs.* 1373 W m^{-2}).

but its highly-re flective, planet encircling, sulfuric acid clouds scatter about 76% of this sunlight back to space before it can be absorbed by the surface or atmosphere [*Moroz*, 1983]. With this high albedo, Venus absorbs about 157 W/m^2, or about 65% as much solar energy as the Earth. To remain in thermal equilibrium, Venus must emit the same amount of energy to space. If Venus emits as a black body, (ϵ = 1) Equation 3 gives an effective globally averaged emission temperature near 230 K. This value is remarkably consistent with results inferred from ground-based infrared observations acquired during the first half of this century, which revealed cloud top temperatures between 225 and 240 K on both the day and night sides of the planet [*Pettit and Nicholson* 1955; *Sinton and Strong*, 1960].

The Thermal Equilibrium Temperature Profile

The preceding results describe only the globally-averaged thermal balance of the surface-atmosphere system.

lc

$$T_s = [2 I_{\odot} (1 - a_s)/\sigma]^{1/4}. \tag{8}$$

Even though this simple example illustrates the basic physics of a solar-driven atmosphere](greenhouse 111(, ('11,1111.111 ll employs several assumptions that are not valid lot Venus. For example on Venus, the solar energy is not deposited primarily at the surface but within the planet-wide H_2SO_4 clouds. The globally-averaged solar flux absorbed ill the Venus surface is only 20.3 W" m^{-2} or about 13% of the total solar flux absorbed by the system. In addition the wavelength dependence of the atmospheric opacity was also over simplified in this simple example. In reality, the Venus atmosphere absorbs and scatters a significant amount of solar radiation. It also

In general, the thermal balance of planetary atmosphere is determined by solving the thermodynamic energy equation [*c.f. Andrews, Holton and Leovy*, 1987]:

$$\frac{\partial T}{\partial t} + \frac{u}{r\cos\phi}\frac{\partial T}{\partial \lambda} + \frac{v}{r}\frac{\partial T}{\partial \phi} + w\left[\frac{\partial T}{\partial z} + \Gamma\right] = Q,$$

$$\frac{\partial \bar{T}}{\partial t} = -\frac{1}{\bar{\rho} c_p}\frac{\partial \bar{F}}{\partial z},$$

where the globally-averaged net heating rate at each level, $\bar{Q}$, has been expressed in terms of the vertical divergence of the horizontally-averaged net fluxes, $\bar{F}$, and the horizontally-averaged atmospheric density, $\bar{\rho}$. Even though the vertical heat advection term $(w\,\partial T/\partial z + \Gamma]$

in Eq. 9) must vanish to satisfy global mass continuity, the globally-averaged net convective heat fluxes are zero if the vertical velocities and temperature variations are (correla[illegible] not an[illegible] sources or sinks). These fluxes have therefore been included on the right hand side of Eq. 10, such that the globally averaged heating rate at each level depends on the vertical divergence of the net radiative, convective, chemical, and latent heat fluxes.

To solve for the globally-averaged equilibrium temperature structure of a planetary atmosphere, 1-D RCE models express Eq. 10 as an initial value problem in finite difference form

$$T_{i+1,j} = T_{i,j} - \frac{\delta t}{\rho_{i,j} c_p} \left[\frac{F_{i,j+1/2} - F_{i,j-1/2}}{z_{j+1/2} - z_{j-1/2}} \right], \qquad (11)$$

where the current time step is denoted with the index, i, and the model levels are indicated with the index, j. This equation requires both initial conditions and a boundary condition on the fluxes at the surface or at the top of the atmosphere. The initial temperature distribution can be chosen at random or derived from available observations. The boundary condition can take the form of a time-dependent relationship describing the surface energy balance (*i.e.* the time-varying surface heat flux), or be specified as a constant at the lowest or highest atmospheric level (*i.e.* the solar flux at the top of the atmosphere, or a constant upward heat flux at the top of the tropopause). The radiative-convective equilibrium temperature structure can then be derived by explicitly marching this equation forward in time [*c.f. Gierasch and Goody* 1968; *Crisp*, 1989] or by employing an implicit iteration scheme, like Newton-Raphson [*c.f. Pollack and Ohring*, 1973; *Ramanathan*, 1976]. In either case, the net fluxes must be evaluated throughout the atmosphere at each iteration. When the atmosphere reaches thermal equilibrium, the net flux divergence vanishes at all levels and this iterative procedure converges.

The various components of the net flux behave differently as the temperature distribution evolves to radiative equilibrium. For Venus, neither latent or chemical heat fluxes are thought to be important to the thermal balance at altitudes below the mesopause (~ 100 km). These quantities will therefore not be discussed further. Convective heat fluxes are assumed to be significant only at levels were the temperature lapse rates exceed the local adiabatic lapse rate. These fluxes can therefore vary substantially as the temperature structure evolves and radiative forcing produces convectively-unstable regions. The globally-averaged solar fluxes and heating rates remain almost constant as the temperature structure evolves, because the total solar insolation changes very [illegible] on Venus, and the atmospheric optical properties are weak functions of temperature. The thermal fluxes and [illegible] rates change much more rapidly as the temperature evolves, because the thermal source function depends strongly on temperature. These contributions to thermal balance are summarized below.

Convective Heat Transport

Convective processes dominate the vertical heat transport throughout much of the lower atmosphere of Venus, which is relatively opaque to thermal radiation [*Pollack*, 1969b]. They are also important within the middle cloud layer, which is heated strongly from below by upwelling thermal radiation, and cools effectively to space from its upper regions [*Pollack et al.* 1980; *Ingersoll et al.* 1987; *Crisp et al.* 1990]. Convection is usually simulated in 1-D RCE models by a simple "convective adjustment" process. In this approach, each time the vertical temperature gradient exceeds the local adiabatic lapse rate in any model layer, enough heat is instantaneously transported from the bottom to the top of the layer to stabilize the lapse rate [*Manabe and Wetherald*, 1967]. Prandl's mixing length theory has also been used to estimate convective fluxes in 1-D RCE models [*Gierasch and Goody*, 1967]. This method is more realistic than convective adjustment because it does not require instantaneous heat transport, but it has not yet been widely used for studies of the Venus thermal balance.

Radiative Heat Transport

[illegible]

$$\mu \frac{dI(\tau,\mu_0,\mu,\phi,\nu)}{d\tau} = I(\tau,\mu_0,\mu,\phi,\nu) - S(\tau,\mu_0,\mu,\phi,\nu), \qquad (12)$$

where τ is the column-integrated optical depth, (measured from the top of the atmosphere), μ is the cosine of the local zenith angle, ϕ is the azimuth angle, ν is the monochromatic wavenumber (cm^{-1}) at which

$$F\uparrow(\tau,\mu_\odot,\nu) = \int_0^{2\pi}\int_0^{1} I(\tau,\mu_\odot,\mu,\phi,\nu)\,\mu\,d\mu d\phi. \tag{14}$$

$$F\downarrow(\tau,\mu_\odot,\nu) = \int_0^{2\pi}\int_0^{-1} I(\tau,\mu_\odot,\mu,\phi,\nu)\,\mu\,d\mu\,d\phi. \tag{15}$$

The total net radiative flux at each level is then determined by integrating these quantities over wavenumber:

$$F_d^{\lambda}(\tau) = \frac{1}{2}\int_0^1 F_d^{\lambda}(\tau,\mu_\odot)d\mu_\odot, \tag{18}$$

to yield the global average net radiative flux at each level, or integrated over a latitude band

$$F_d^{\lambda}(\tau,\lambda) = \frac{1}{2\pi}\int_0^{\pi} F^{\lambda}[\tau,\mu_\odot(\lambda,\phi')]d\phi'. \tag{19}$$

to give the diurnally-averaged net radiative flux at latitude, λ.

Several accurate numerical methods have been developed to solve these equations [*c.f. Goody and Yung*, 1989], but these methods are still not widely used for thermal balance calculations because they are too computationally demanding. The principal problem is that these equations describe the fluxes for a specified monochromatic spectral point, ν, solar zenith angle, $\mu_\odot$, temperature distribution, $T(z)$, and optical depth distribution, τ. For 1-D RCE models, radiative fluxes are needed at wavenumbers throughout the solar and thermal spectra, as well as for a range of solar zenith angles, temperature profiles, and optical depth distributions. In addition, for thermal balance calculations, these radiative fluxes must be re-evaluated many times as the derived thermal structure evolves.

The spectral resolution is determined by the requirement that the solar and thermal source functions and all significant atmospheric and surface opacity variations be completely resolved. The thermal source function and the optical properties of the surface and airborne particulates change relatively slowly with wavenumber, such that a few hundred points would be adequate to resolve their spectra. The spectra of absorbing gases can vary much more rapidly, however. For example, there are hundreds of thousands of CO_2 and H_2O vibration-rotation lines that contribute significant opacity of the Venus atmosphere at *(iii)* employ assumptions about the , ngul ar dependence of the radiation field (*e.g.* two stream or δ Eddington methods) These methods (i m dramatically improve the efficiency of 1 1) RCE models, but they can also introduce errors that compromise their results The principal approximations employed in each thermal balance study are described in Sections IV and V.

111. TEMPERATURES ANI) OPTICAL

water vapor mixing ratios between < 0.5 ppmv and 10 ppmv [*Barker*, 1975] but the *PV* Orbiter Infrared Radiometer (OIR) detected mixing ratios more than twice this large (1 (10-t 40 ppmv) at mid latitudes in the mid-afternoon

SO_2 has a strong rotation band in the far infrared (< 1.")() cm^{-1}), and vibration rotation fundamentals centered near 1151.7 (ν_1), 517.75 (ν_2), and 1362 (ν_3). It also has significant overtone bands near 2500 and 4050 cm^{-1} This gas is the principal source of opacity at near-UV wavelengths between 30000 and 50000 cm^{-1} (0.2 and 0.33 μm). SO_2 mixing ratios vary with altitude, and time [*Esposito et al* 1988]. PV entry probe observations indicate mixing ratios < 600 ppmv at 52 km, >170 ppmv at 42 km, and 185 ± 43 ppmv at 22 km. The *Venera 12* Gas Chromatograph measured values near 130 ± 35 at 22 km [*c.f. von Zahn et al* 1983, in **Venus**]. Recent near-infrared observations support these results, indicating values near 130 ± 40 near the cloud base [*Bézard et al* 1993]. Above the clouds, SO_2 mixing ratios near 0.1 ppmv were detected in the late 1970's by ground-based observers [*Barker*, 1979], and instruments on the *PV* Orbiter [*Esposito et al.* 1979], but the abundance of this gas above the cloud tops has decreased by about an order of magnitude

atmosphere
Aerosol opacity

to the upper (1011(1 layer III most thermal balance studies, this unknown UV absorber is included as an impurity in the *Mode / particles* at levels within the upper Cloud I'(J do II is. the single scattering albedos of III(,S(particles are 1{, (111 ((7(1 at near UV wavelengths by the amounts needed to produce the observed spectrally dependent geometric albedo of Venus [*cf. Crisp*, 1986]

IV. THERMAL BALANCE OF THE DEEP ATMOSPHERE

Much of the early work on the thermal balance **of** the deep atmo S[)11(,1'(, was reviewed by *Tomasko* in **Venus**. That work will therefore only be briefly summarized here to set the stage for subsequent observational and modeling studies. We will then review recent observational studies that have provided improved constraints on the thermal structure, the distribution of solar and thermal radiation, and this high altitude emission should produce a limb brightened disk. I III. constraint ('(1111(1 not be tested (111 ('('1/'! from the }',IO1III (1, however, because the microwave instruments available at that 11111 ((11(1 not provide the spatial resolution needed to resolve the Venus disk. 1 he *Mariner 2* flyby (II" Venus in December of 1962 provided the first opportunity 1(I test this hypothesis. Its high spatial resolution microwave observations showed that the Venus disk was limb darkened at wavelengths near 1.0("111. 'I'II('S(`1(sults largely precluded the ionospheric origin for the high brightness temperatures.

Both observations and theoretical [[10(dels of the Venus atmosphere evolved substantially by 1967, when *Venera 4* entered the

flew

were 11111 ('11 larger than those inferred from existing ",[[) 111)(1 based observations [*Kuiper et al.* 1969; *Belton and Hunten* 1966]. *Venera 4* observations provided a tentative detection of water vapor below the clouds, but existing ground based infrared spectroscopic observations appeared to 1)1' ('('111(1(' water as a major con 11(111' ent of the ('1011(1s. If the ('10(1(1s were not composed of water, they might not be sufficiently transparent at visible wavelengths, or sufficiently opaque at thermal wavelengths to produce the 11(/1111(,(1 greenhouse warming.

Ground-based and spacecraft observations made in the early 1970's provided new information about the thermal balance of the Venus atmosphere. Ground-based spectroscopy [}'(ll/ //(/ I 973; *Pollack et al.* 1974] and polarimetry [*Hansen and Hovenier* 1974] showed that the ('1011(1s were co111105('(1 of concentrated H_2SO_4 droplets, with modal radii near 1μm. *Venera 8* solar flux measurements confirmed that some of the incident sunlight penetrated to the surface of Venus, and that the water vapor below the clouds (100 to 1000 ppm) than that assumed in earlier greenhouse models (> 3000 ppmv), but the reduced water opacity was largely compensated by CO_2 pressure induced bands and the strong SO_2 vibration-rotation fundamentals at mid-infrared wavelengths, which were neglected in the earlier models. The *PV* measurements also showed that the H_2SO_4 clouds provided less thermal opacity than earlier greenhouse models had assumed. *Pollack et al.* [1980] found that the observed cloud particle populations did not provide enough thermal opacity to maintain the observed thermal structure, and postulated the presence of large numbers (> 10^5 particles cm^{-3}) of tiny, ($r_{eff} \leq 0.07\mu m$) "Mode 0" particles in the upper cloud. With this opacity, they were able to simulate the high surface temperatures, and many other features of the observed thermal structure including the stable region near the base of the clouds, and the neutrally-stable region within the middle cloud.

Shortcomings of Existing Greenhouse Models

Pollack et al. [1980] added significantly to our understanding of the deep atmosphere thermal balance, but limitations in the input data and modeling methods precluded a definitive description of the Venus greenhouse. One of the most often quoted concerns is that this model required large numbers of "invisible" *Mode 0* particles to reproduce the observed thermal structure when the nominal (*Venera 11/12*) H_2O abundances were used [*Tomasko* 1983]. Even though the presence of these particles could not be precluded by the *PV* Large Probe Cloud Particle Spectrometer (LCPS) observations, the apparent need for any undetected opacity source compromises our understanding of the thermal balance, however.

Uncertainties in the H_2O mixing ratios below the clouds have also [illegible] by these gase[illegible] to the thermal [illegible]rticular, diffe[illegible]ent instruments [illegible]ter vapor abun[illegible]dances that var- [illegible]imilar altitud[illegible]s. *Pollack et al.* [illegible]photometer r[illegible]sults, which de- [illegible] 20 ppm at the [illegible]surface, as their [illegible] Gas Chrom[illegible]tograph results [illegible]ofile. No tests [illegible]were performed [illegible]onditions, but [illegible] comparisons of [illegible]" profiles sug[illegible]gest that water [illegible]alues used her[illegible] would not pro- [illegible]ce the observe[illegible]l temperatures. [illegible] calculations [illegible]eported by *Pol-* [illegible]ed by approxi[illegible]ations adopted [illegible]e empirical ba[illegible]nd absorptance [illegible] by CO_2, H_2O,[illegible] and SO_2 at infrared wavelengths can introduce 10% errors for pressures and absorber pathlengths beyond those used to fit their empirical coefficients [c.f. *Crisp et al.* 1986]. Other errors were introduced by shortcomings in the knowledge of the absorption by gases at high temperatures and pressures, like those encountered in the deep atmosphere of Venus.

The neglect of multiple scattering at all thermal infrared wavelengths contributes another source of error. This simplification will produce negligible errors at wavelengths where H_2SO_4 aerosols have very low single scattering albedos. But it could produce significant errors at wavelengths near 5 and 12μ where *Mode 3* particles have single scattering albedos near 0.6. It was not impossible to evaluate these errors until recently because of the computational

$$T_s = [2I_{\odot}(1 - a_s)/(1 - r)\sigma]^{1/4}. \qquad (22)$$

86–100 at the cloud tops (~68 km), to ~1 K day^{-1} at the base of the upper cloud. The heating at these levels is associated primarily with the absorption of UV radiation by the unknown cloud-top UV absorber. LSFR observations indicate that this absorber is confined to altitudes above the base of the upper cloud. Within the middle and lower clouds, the globally averaged heating rates decrease from 0.19 K day^{-1} at 55.3 km to 0.52 K day^{-1} at 48.9 km. Below the clouds, the globally averaged heating rate continue to decrease monotonically to values near 0.008 K day^{-1} at 36.1 km and 0.001 K day^{-1} at the surface. The computed globally averaged solar flux at the surface is 17 W m^{-2}, or about 2.6% of the incident solar flux.

The *PV* Small Probe Net Flux Radiometers (SNFR) and Large Probe Infrared Radiometer (LIR) were designed to provide detailed vertical profiles of the net thermal fluxes throughout the deep atmosphere, but their preliminary results included large errors that initially lead to confusion [*Suomi et al.* 1980; *Ingersoll and Pechmann*, 1980] and seriously compromised their value for thermal balance studies. *Revercomb et al.* [1985] reanalyzed these measurements, identified plausible sources for the measurement errors, and derived "corrected" fluxes for both the SNFR and LIR instruments. These results were then analyzed with a radiative transfer model, (based on *Pollack*, 1969a]), to yield new constraints on the cloud particle populations, the global distribution of water vapor, and the thermal cooling rates in the deep atmosphere. They found that the *Mode 3* number densities in the lower cloud inferred from the LCPS observations were 1 (Sounder Probe) to 5 (North Probe) times larger than those indicated by the observed net thermal fluxes if these particles were composed of 75% H_2SO_4 vapor. This reanalysis also confirmed earlier SNFR results [*Suomi et al.* 1980], which suggested that an additional source of thermal opacity was needed in the upper cloud (58–71 km). This opacity could be supplied by the sub-micron *Mode 0* particles, or by enhancing the number density of *Mode 2*

Regardless of their origin, the meridional [illegible] in net thermal [illegible] inferred from the SNFR and LIR observations have direct implications for the thermal balance and dynamics of the deep atmosphere [*Revercomb, et al.* 1985]. Because the net solar fluxes are [illegible] to decrease with latitude, the observed net thermal flux increase with latitude suggests that the deep atmosphere is not in local radiative-[illegible]. Large-scale dynamical processes must therefore transport a significant amount of heat between low and high latitudes in these levels. A conventional, equator-to-pole Hadley cell might provide the meridional heat transport needed to balance the observed variations in the net radiative cooling [*Gierasch*, 1975; *Schubert*, 1983; *Hou and Goody*, 1985]. This cell would produce rising motion at low latitudes, poleward flow near the top of the domain (cloud tops?) descending motion at high latitudes, and equatorward flow at depth. Because the temperature lapse rates are moderately stable throughout much of the lower atmosphere, the rising motion at low latitudes will be associated with adiabatic expansional cooling. Similarly, adiabatic compressional heating will occur in the descending, high-latitude branch of this cell. The net dynamical heating produced by this cell could therefore compensate for the horizontal variations in net radiative heating.

VEGA Balloon and Lander Measurements

On June 11 and 15, 1985, the Soviet *VEGA* mission deployed surface landers and meteorological balloons in the Venus atmosphere. The two *VEGA* balloons entered the atmosphere near local midnight and collected data for about 48 hours each as they were transported beyond the morning terminator by the prevailing east-west winds. Even though they were inserted at similar latitudes (7° 11' N and 6° 28' respectively), the two balloons sampled air masses separated by about 135° of longitude. Each balloon acquired *in situ* measurements of pressure, temperature, vertical wind velocity, cloud density, ambient illumination, and the frequency of lightning for about 48 hours as it floated at altitudes between about 50 and 54 km, within the middle cloud [*Sagdeev et al.* 1986].

The *VEGA Balloon* measurements revealed several surprising features of the thermal structure and dynamics of the middle cloud layer. First, even though the observed temperature lapse rates were near adiabatic (stability ranging from 0 to 2 K/km), as was expected from earlier *PV* and *Venera* observations, the air masses sampled by the two balloons had temperature profiles that were offset by 6.5 K [*Seiff et al.* 1987]. The amplitude of this temperature difference was surprising because it is comparable to the pole-to-equator gradient at these altitudes. In addition, [illegible] balloons encountered vertical winds with amplitudes sometimes exceeding 3 m/s. Comparisons of observed temperatures and winds revealed upward convective heat fluxes between

0 and 360 W m . but the mean value for both balloons was 40 W" m . This is comparable to the globally-averaged downward solar flux at these levels. These data confirm that convection 1. responsible for the majority of the vertical heat transport through the middle cloud

The *VEGA 2* Lander provided the first high resolution measure-111(nts of the atmospheric temperature S111)([111[, near

spelling error

X

1985 These features might be associated with the ... branch of a cloud level Hadley circulation [*Crisp et al.* 1991b

Finally NIR observations at wavelengths between 1.0 and 1.18 μm have been used to constrain the temperature lapse rates near the Venus surface. Comparisons between synthetic radiance maps and spectral image cubes acquired during 1991 indicate night-side averaged temperature lapse rates of 7 to 7.5 K/km in the lowest 6 km [*Meadows and Crisp*, 1996]. These lapse rates indicate much greater static stability than those inferred from earlier measurements and greenhouse models (s to 8.5 K/km) [*c.f. Seiff* 1983; *Seiff et al* 1987] If confirmed by subsequent observations, these results might indicate the presence of significant radiative losses from the surface during the Venus night

Recent Advances in Radiative Transfer Modeling Methods

Additional insight into the thermal balance of the deep atmosphere has been provided through the development of progressively more sophisticated and reliable numerical radiative transfer models In the late 1970's. when the last comprehensive investigations of the deep atmosphere were conducted, the approximations and simplifications required for computational efficiency (empirical band models, two stream solutions to the equation of transfer, neglect of scattering processes at thermal wavelengths) substantially limited the reliability and range of validity of even the most sophisticated models. Their accuracy was further limited by uncertainties in the optical properties of gases at high temperatures and pressures. Recent advances in our understanding (an)i traints on the opac-

sing. or plural?

algorithm (c.f. *Bézard et al* 1990 *Crisp et al* 1991a b

Consistency!
Some places you hypherate, others you don't

m^{-2}. These flux reductions are remarkably similar to those obtained by adding *Mode 0* particles to the upper cloud [*Pollack et al.* 1980; *Suomi et al.* 1980]. In spite of its large impact on the thermal fluxes at the top of the atmosphere, the neglect of multiple scattering at thermal wavelengths produces no cooling rate errors larger than about 10% in the deep atmosphere (Figure 5).

The nominal atmospheric H_2O profile used in these calculations has a mixing ratio of 30 ppmv between the surface and the cloud base [*Pollack et al.* 1993; *Bézard et al.* 1995]. To determine the effect of much larger water vapor abundances, like those adopted in earlier greenhouse models, fluxes and heating rates were computed with the *Venera* 11/12 Spectrophotometer profile [*Moroz et al.* 1978], which was adopted as the nominal profile by *Pollack et al.* [1980] (Figures 4 and 5). The largest flux differences are seen at wavenumbers less than 300 cm^{-1}, in the strong H_2O rotation band, and within the strong water vibration-rotation bands centered near 1580 and 4000 cm^{-1}. Somewhat surprisingly, the net spectrally-integrated difference between the fluxes at the top of the at assensitive 10 these (loud optical depth changes. the net effe l of a 50% decrease in the cloud partic le dens ity is to increase the net radiative heating throu ghout the upper cloud (0 6 to 0 028 ba r) by 0.6 K/day, and increase the net radiative coo ling in the middle and lower clouds by about 0.2 K/day. These resu lts suggest that long lived variations in the cloud pa rticle number densities like those inferred from ground - based NIR observations (If the night side, could pro duce temperature variati ons within the middle and lower clo uds as large as those observed by the two *VEGA* Balloons If this were the case, the warmer temper- atures measured by *VEGA Balloon 1* suggest s that it may have floate (I in an air mass where the clouds were more dense, while the the cooler *VEGA Balloon 2* profile suggests I hat it floated in a less den se region of the clou d. This conclusion is supported by the available cloud density observa tions obtained by that mission. The nephelometer carr ied by *VEGA Balloon 1* recor ded some of 1 he highest particle densit ies ever seen within the Venus clouds [*Ragent et al.* 1987]. '1 he nephelometer did not wor k on t he second *VE GA Balloon*, but the *VEGA 2* Lande r cloud Par ticle Experiment detected very few large par t icles wit hin the middle and lower clouds [*Moshkin et al.* 1986].

where?

V. THERMAL BALANCE OF THE MESOSPHERE

The pioneering study of the the rmal balance of the Venus meso sphere was conducted by *Dickinson* [1 972]. In that investigation, the globally-averaged radiative equilibr ium temperature st r ucture was de- rived at altitudes between 66 and 130 km for a pure CO_2 atmosphere. The radiative transfer mo del included the effects of non-local thermo- dynamic equilibrium, but did not include a rigorous treatmer rotating cloud - top zonal winds would continue to accelerate at meso spheric levels (to values as high

le

e. «

diative forcing were not yet identified in the early 1980's when *Taylor et al.* [19 3] reviewed this topic in Venus. In their review, they proposed that the high polar mesospheric temperatures might be produced by *i* compressional heating in the descending branch of an axially-symmetric, equator-to pole Hadley cell, *(ii)* enhanced high latitude solar heating associated with increases in the atmospheric path lengths and abundances of (optically-thin) polar mesospheric aerosols, *(iii)* the absorption of the intense upwelling thermal radiation emitted by the polar hot spots by CO_2 and aerosols at mesospheric levels, or some combination of these])[()('(%s(%. Subsequent modeling studies have shown that none of these mechanisms can account for the observed thermal [redacted] tions between the vertically-propagating atmospheric thermal tides and the zonal superrotation [*Fels and Lindzen* 1974; *Baker and Leovy* 1987; *Newman and Leovy*, 1992]. These studies are described in the next two subsections.

Radiative Forcing of the Mesosphere

In spite of the radiatively anomalous nature of the observed mesospheric thermal structure, radiative forcing was implicated in two of the three mechanisms proposed for maintaining this feature. [*Crisp*, 1983; 1986; 1989] developed a radiative-convective-equilibrium (RCE) [110(1 ('1 10 provide a more detailed are (missing a word, ?

found that the observed thermal structure could be maintained in the presence of the nominal radiative forcing by meridional cell with upward vertical velocities < 1 cm s^{-1} at low latitudes, poleward velocities of ~ 10 m s^{-1} at altitudes near the mesopause, downward vertical velocities of < 2.3 cm s^{-1} at high latitudes, and a weak ~1 m s^{-1} equatorward flow at altitudes between 60 and 64 km (Figure 10).

Because this meridional circulation cell is thermodynamically indirect (i.e. it is not a consequence of hot air rising and cold air sinking, like a Hadley cell), it must be driven by an external momentum source. *Crisp*, [1983, 1989] proposed that this forcing could be provided by the interaction between the vertically propagating atmospheric thermal tides generated at the cloud tops and the mean zonal super-rotation [*c.f. Fels and Lindzen*, 1974]. In these models, the tides generated within the upper cloud deck (57 to 71 km) propagate to higher mesospheric levels (80 to 100 km), where they are strongly damped by radiative cooling [*Crisp* 1983; 1989]. This radiative damping causes the tides to transfer their momentum to the zonal flow at these levels. Because the tides have phase speeds near 4 m/s (prograde), they act as source of drag on the strong (~ 100 m s^{-1}) retrograde zonal super-rotation at their damping altitudes. This tidal drag decelerates the super-rotation in the upper mesosphere and forces a thermo

[redacted]

comprehensive, simultaneous, global description of the thermal structure and optical properties of the mesosphere. This instrument collected more than 1500 moderate-resolution (5 to 7 cm^{-1}) thermal infrared (270 to 1650 cm^{-1}) spectra at latitudes between 60° S and 87° N. These spectra were analyzed to retrieve a self-consistent description of the thermal structure, aerosol distribution, and SO_2 mixing ratios at altitudes between 60 and 90 km [*Zasova and Moroz*, 1992].

The *Venera 15* temperatures and aerosol distributions were also used to derive solar heating rates and thermal cooling rates at mesospheric levels [*Schafer et al.* 1990; *Haus and Goering*, 1990; *Titov*, 1995]. Their solar radiative transfer model incorporated the *Modified Eddington* approximation [*Meador and Weaver* 1980] and the 2-stream *Adding* method [*Lacis and Hansen*, 1974; *Crisp*, 1983; 1986] to find solar fluxes and heating rates in the presence of gas and aerosols absorption and scattering. A line-by-line model was used to derive the monochromatic optical properties of gases. Unlike in earlier thermal balance models, these investigators derived thermal fluxes from a model that could accommodate multiple scattering as well as absorption by gases and aerosols (successive orders of scattering) [*Schäfer et al* 1990]

The *Venera 15* thermal balance studies confirm that the solar heating rates in the lower mesosphere (60 to 70 km) depend strongly on the assumed distribution of the H_2SO_4 aerosols and the UV absorber near the cloud top. The nominal aerosol models adopted by *Haus and Goering*, [1990] have larger H_2SO_4 aerosol and UV absorber optical depths at levels above 65 km than those inferred from *PV* observations [*Tomasko et al.* 1980; 1985; *Crisp*, 1983, 1986]. Because of this, *Haus and Goering* find solar heating rates at levels between 65 and 73 km that are 2-3 K day^{-1} larger than those derived in the earlier studies. At altitudes above 73 km, *Haus and Goering*, [1990] find solar heating rates that are significantly lower than those derived in the earlier studies. These heating rate differences are most likely caused by the use of different CO_2 absorption line databases. While *Haus and Goering* used line parameters from the 1976 version of the AFGL line catalog [*Rothman et al.* 1976], *Crisp*, [1983, 1986] used values from the 1980 version of this database [*Rothman*, 1981], which included a more complete description of the weak near-infrared overtone bands at wavelengths less that 2.15 μm. The absorption of sunlight in these bands dominates the near-infrared heating rates at most mesospheric levels. *Haus and Goering*, [1990] also find that the thermal cooling rates depend strongly on the distribution of aerosols in the upper cloud, but these cooling rates are much less sensitive to the neglect of multiple scattering, or the abundance of H_2O.

Even though the latitude-dependent solar heating and thermal cooling distributions derived by *Haus and Goering*, [1990] are qualitatively similar to those obtained from *PV* observations [*Crisp* 1983; 1986; 1989], the net radiative heating rates are significantly different. *Crisp* found net radiative heating at latitudes equatorward of ~ 40° and net radiative cooling at higher latitudes at most mesospheric levels. This net heating distribution indicates that the mesosphere is roughly in global radiative equilibrium at each sistent with the results derived from *PV* observations by *Crisp* 1983, 1989. However, *Titov* finds that net cooling also prevails at low latitudes above the cloud tops, while *Crisp* finds net heating there.

Temporal Variations in the

reasonably well understood. Groundbased and spacecraft observations acquired since the late 1970s combined with improved modeling methods have largely confirmed that the thermal balance of the deep atmosphere is maintained by an efficient atmospheric greenhouse mechanism. The warm polar mesosphere has been attributed to the presence of a thermodynamically indirect meridional circulation cell that is driven by interactions between atmospheric thermal tides and the zonal super-rotation. However, there are several other aspects of the Venus thermal structure and thermal balance that are not yet well understood. For example, we still know very little about the thermal structure in the lowest atmospheric scale height, and we have no direct measurements of temperatures poleward of 60°. The radiative and dynamical processes associated with the large scale variations in thermal structure and cloud particle number densities in the middle and lower cloud are largely

add a NASA acknowledgment here

REFERENCES

Barker, E. S. Observations of Venus water vapor over the disk of Venus: The 1972–1974 data using the H_2O lines at 8197 øA and 8176 øA. *Icarus*, 25:268–281, 1975.

Galileo infrared imaging spectroscopy measurements at Venus. *Science*, 253:1541–1548, 1991.

Chapman, S. and R. S. Lindzen. Atmospheric Tides. Reidel, Dordrecht, Netherlands, 200 pp, 1970.

Clancy, R. T. and D. O. Muhleman. Long-term (1979–1990) changes in the thermal, dynamical, and compositional structure of the Venus mesosphere as inferred from microwave spectral line observations of ^{12}CO, ^{13}CO and $C^{18}O$. *Icarus*, 89:129–146, 1991.

Clough, S. A., F. X. Kneizys, E. P. Shettle, and G. P. Anderson. Atmospheric radiance and transmission: FASCOD2. *Sixth Conference on Atmospheric Radiation*, pp. 141–144, Williamsburg, VA. Amer. Meteorol. Soc., Boston, 1986.

Connes, P., J. Connes, W. S. Benedict, and L. D. Kaplan. Traces of HCl and HF in the atmosphere of Venus. *Ap. J.*, 147:1230–1237, 1967.

Crisp, D. *Radiative forcing of the Venus mesosphere*, Ph.D. Thesis, Princeton University, 1983.

Crisp, D. Radiative forcing of the Venus mesosphere. I. Solar fluxes and heating rates. *Icarus*, 67:484–514, 1986.

Crisp, D. Radiative forcing of the Venus mesosphere. II. Thermal fluxes, cooling rates, and radiative equilibrium temperatures. *Icarus*, 77:391–413, 1989.

Crisp, D., S. B. Fels, and M. D. Schwarzkopf. Approximate methods of finding CO_2 15 μm band transmission in planetary atmospheres. *J. Geophys. Res.*, 91(D11):11851–11866, 1986.

Crisp, D., W. M. Sinton, K. Hodapp, B. Ragent, F. Gerbault, J. Goebel, R. Probst, D. Allen, and K. Pierce. The nature of the near infrared features on the Venus night side. *Science*, 246:506–509, 1989.

Crisp, D., A. P. Ingersoll, C. E. Hildebrand, and R. A. Preston. VEGA Balloon meteorological measurements. *Adv. Space Res.*, 10:(5)109–(5)124, 1990.

Crisp, D., D. A. Allen, D. H. Grinspoon, and J. B. Pollack. The dark side of Venus: Near-infrared images and spectra from the Anglo-Australian Observatory. *Science*, 253:1263–1266, 1991a.

Crisp, D., S. McMuldroch, S. K. Stephens, W. M. Sinton, B. Ragent, K. W. Hodapp, R. G. Probst, L. R. Doyle, D. A. Allen, and J. Elias. Ground-based near-infrared imaging observations of Venus during the Galileo encounter. *Science*, 253:1538–1541, 1991b.

de Bergh, C., B. Bézard, T. Owen, D. Crisp, J. P. Maillard, and B. L. Lutz. Deuterium on Venus: Observations from Earth. *Science*, 251 -15 , 19,1991

deBergh C, B Bézard D Crisp, J P. Maillard, T Owen J Pollack and D Grinspoon Water in the deep atmosphere of Venus from high resolution spectra of the night side *Adv. Space Re*, 15 (4)79 (4)88, 1995.

Dickinson, R. E. Infrared radiative heating and cooling in the Venusian mesosphere. I. Global mean radiative equilibrium. *J. Atmos. Sci.*, 29:1531 1556, 1972.

Diner D. J., J. A Westphal, and F. P. Schloerb. Infrared imaging of Venus s I I micrometers. *Icarus*, 27:191 195, 1976

Donahue, T M and R. R. Hodges, Jr. Past and present water budget of Venus J. *Geophys. Res.*, 97(E4):6083 6091. 1992.

Donahue, T M , J. H. Hoffman, R. R Hodges, Jr , and A J. Watson. Venus was wet: A measurement of the ratio of deuterium to hydrogen *Science* 216:630 633, 1982

Drake, F D. 10-cm observations of Venus near superior conjunction. *Nature*, 195 :894, 1962.

Drossart, P., B.Bézard, Th. Encrenaz, E. Lellouch, M.Roos, F. W. Taylor, A. D. Collard, S. B. Calcutt, J. B. Pollack, D. H. Grinspoon, R.W. Carlson, K. H. Baines, and L. W. Kamp. Search for spatial variations of the H_2O abundance in the lower atmosphere of Venus from NIMS-Galileo. *Planet. Space Sci.*, 41 (7):495 504,1993.

Esposito, L. W. Sulfur dioxide: episodic injection shows evidence for active Venus volcanism. *Science*, 223:1072 1074, 1984.

Esposito, L. W., J. R. Winick, A. I. F. Stewart. Sulfur dioxide in the Venus atmosphere: Distribution and implications. *Geophys. Res. Lett.*, 6:601 60 1, 1979.

Esposito, L. W., M. Copley, R. Eckert, L. Gates, A.I.F. Stewart, and H. Worden. Sulfur dioxide at the Venus cloud tops, 1978 1986. *J. Geophys. Res.*, 93, 5267 5276, 1 988.

Fels, S. B. An approximate analytical method for calculating tides in the atmosphere of Venus *J. Atmos. Sci.*, 43:2757, 1986.

Fels, S. B., and R. S. Lindzen. The interaction of thermally excited gravity waves with mean flows. *Geophys. Fluid Dyn* 6 149 192, 1974

Fels, S. B., J. T. Schofield, and D Crisp, Observations and theory of the solar semidiurnal tide in the Venus mesosphere. *Nature*, 312: 431 434, 1984

Gierasch, P. and R Goody A study of the thermal and dynamical structure of the Martian lower atmosphere. *Planet Space Sci* 16, 615 646, 1968

Goody, R. M. and Y. L. Yung. *Atmospheric Radiation Theoretical Basis*. 2nd Edition Oxford University Press 519pp 1989.

Goody, R. M. and A. R. Robinson. A discussion of the deep circulation of the atmosphere of Venus. *Astrophys. J.* 146:339 355, 1966.

Grinspoon, D. H., J. B Pollack B R Sitton R W Carlson, L. W. Kamp, K. H. Baines Th Encrenaz, and F. W. Taylor. Probing Venus's cloud structure with Galileo NIMS *Planet. Space Sci.*, 41(7):515 542, 1993

Hansen, J. E., and J. W. Hovenier Interpretation of the polarization of Venus. *J. Atmos. Sci* 31:1137 1160, 1974

Hansen, J. E., and S. Matsushima The atmosphere and surface temperature of Venus a dust insulation model *Astrophys. J.*, 150:1139 1157, 1967

Haus, R., and H. Goering Radiative energy balance of the Venus mesosphere. *Icarus*, 84: 62 82, 1990.

Herries, J. E. The temperature variation of the far infrared absorption in compressed CO_2 *J Phys Sci. B: Atom. Molec. Phys.*, 3:704, 1970.

Hoffman, J. H., R. R. Hodges, T. M Donahue, and M. B. McElroy. Composition of the Venus lower atmosphere from the Pioneer Venus Mass Spectrometer. *J Geophys. Res.*, 85(A13):7882 7891, 1980.

Hou, A. Y., and R. Goody. Diagnostic requirements on the superrotation on Venus. *J. Atmos. Sci* 42:413 432, 1985.

Howard, T.

Kliore A. J. Changes in the structure and dynamics of the Venus middle atmosphere. *Bull. Amer. ... Soc.* 26 1147, 1994

Kliore, A. J., G. S. Levy, D. L. Cain, G. Fjeldbo, S. I. Rasool. Atmosphere and ionosphere of Venus from the Mariner 5 S band radio occultation measurement. *The Venus Atmosphere*, (R. Jastrow and S. I. Rasool eds.), Gordon and Breach, New York, pp 105 127, 1969

Kliore, A. J and I. R. Patel. Thermal structure of the atmosphere of Venus from Pioneer Venus radio occultations. *Icarus*, 52:320 331, 1982.

Knollenberg, R. G., L. Travis, M. Tomasko, P. Smith, B. Ragent, L. Esposito, D. McCleese, J. Martonchik, and R. Beer. The clouds of Venus: A synthesis report. *J. Geophys. Res.*, 85(A13):8059 8081, 1980

Knollenberg, R. G., and D. M. Hunten. The microphysics of the clouds of Venus: Results of the Pioneer Venus particle size spectrometer experiment. *J. Geophys. Res.*, 85(A 13):8038 8058, 1980.

Kuiper, G. P., F. F. Forbes, and J. L. Johnson. Program of astronomical spectroscopy from aircraft. *Comm. Lunar Plan*

Kuz'min, A. D., and A. E. Salomonovich. Observations of the radio emission of Venus and Jupiter at wavelength 8 cm. *Astron. J.*, 39:660 668, 1962.

Meadows, V. S. and D. Crisp. Ground-based near-infrared observations of the Venus nightside: The thermal structure and water abundance near the surface. *J. Geophys. Res.* 1996 in press.

Meadows, V. S. *Infrared Observations of Venus with IRIS.* Ph.D Thesis, University of Sydney, 1994.

Moore, J. F. Infrared absorption of carbon dioxide at high densities with application to the atmosphere of Venus. *Rep. X-630-72-48*, NASA Goddard Space Flight Center, Greenbelt, Md., 1971.

Moroz, V. I., B. E. Moshkin, A. P. Ekonomov, N. F. San'ko, N. A. Parfent'ev, and Yu. M. Golovin. Spectrophotometric experiment on board the Venera-11, -12 descenders: Some results of the analysis of the Venus day-sky spectrum. *Space Res. Inst. Acad. Sci. Leningrad* 1978.

Moroz, V. I. Summary of preliminary results of the Venera 13 and Venera 14 missions. *Venus*, (D. M. Hunten, L. Colin, T. M. Donahue, and V. I. Moroz, Eds.), Univ Arizona Press, Tucson, 45-68, 1983.

Moshkin, B. E., V. I. Moroz, V. I. Gnedykh, A. V. Grigor'ev, L. V. Zasova, and A. P. Ekonomov. Vega 1, 2 optical spectrometry of Venus atmospheric aerosols at the 60-30 km levels: preliminary results. *Sov. Astron. Lett.*, 12(1):36-39, 1986.

Na, C. Y., L. W. Esposito, W. E. McClintock, and C. A. Barth. Sulfur dioxide in the atmosphere of Venus, II. Modeling results. *Icarus*, 112:389-395, 1994.

Newman, M., and C. B. Leovy. Maintenance of strong rotational winds in Venus' middle atmosphere by thermal tides. *Science*, 257:647-650, 1992.

North, G. R., R. F. Cahalan, and J. A. Coakley, Jr. Energy balance climate models. *Rev. of Geophys. and Space Phys.*, 19:91-121, 1981.

Öpik, E. J.

far line wings of the [illegible] *J. Quant. Spectrosc. Radiat. Transfer*, 12:31 [illegible] 1989.

Pettengill, G. G., P. G. Ford and R. J. Wilt. Venus surface radiothermal emission as observed by Magellan. *J. Geophys. Res.*, 97(E8): 13091 13102 1992.

Pettit, E., and S. B. Nicholson. Temperatures on the bright and dark sides of Venus. *Publ. Astron. Soc. Pacific* 67: 293 303, 1955.

Pinkley, L. W., and D. Williams. Infrared optical properties of sulfuric acid at 250 K. *J. Opt. Soc. Am.* 66:122 1? 1. 1976.

Pollack, J. B. Temperature structure of nongray planetary atmospheres. *Icarus*, 10:301 313. 1969a.

Pollack, J. B. A non-gray CO_2 H_2O greenhouse model of Venus. *Icarus*, 10:314 341, 1969b.

Pollack J. B., and C. Sagan. The infrared limb darkening of Venus. *J. Geophys. Res.*, 70 [illegible] 103 [illegible] 126. 1965.

Pollack, J. B and G. Ohring. A numerical method for determining the temperature structure of planetary atmospheres. *Icarus*, 19:34-42, 1973.

Pollack, J. B., E. F. Erickson, F. C. Witteborn, C. Jr. Chackerian, A. L. Summers, W. Van Camp, B. J. Baldwin, G. C. Augason, and L. J. Caroff. Aircraft observations of Venus' near-infrared reflection spectrum: Implications for cloud composition. *Icarus*, 23:826, 1974.

Pollack, J. B., and R. Young. Calculations of the radiative and dynamical state of the Venus at

Ramanathan, V., and R. D. Cess. Radiative transfer within the mesospheres of Venus and Mars. *Astrophys. J.* 188

Sagan, C. The planet Venus. *Science*, 133:849–858, 1961.

Sagan, C., K. M. Siegel, and D. E. Jones. On the origin of the Venus microwave emission. *Astron. J.*, 66:52, 1961.

(D. M. Hunten. L. Colin. T. M. Donahue and V. I. Moroz. Eds.), Univ. Arizona Press. Tucson 650 680. 1983.

Titov. D. V. Radiative balance in the mesosphere of Venus from the Venera 15 infrared spectrometer result *Adv. Space Res* 15:(4)73 (4)77 1'1')")

Tomasko, M. G., L. R. Doose and P. H. Smith Absorption of sunlight in the atmosphere of Venus *Science*. 20 :80 82, 1979

Tomasko, M. G., L. R. Doose. P. H. Smith. and A. P. ()(1(' 11. Measurements of the flux of sunlight in the atmosphere of Venus. J. *Geophys. Res.*, 85 8 167 8 186, 1980

Tomasko, M. G. The thermal balance of the lower atmosphere of Venus *Venus*, (D). M. Hunten. L. ('01111. 1 M Donahue. and V. I. Moroz, Eds.),

FIGURE CAPTIONS

Figure 1. Temperature structure of the Venus lower atmosphere from the Pioneer Venus Sounder Probe (solid), and the VEGA 2 Lander ( ). The Pioneer Venus probes transmitted no data between the surface and 12 km (from Seiff et al. 1987)

Figure 2. Static stability (dT/dz + Γ) of the Venus lower atmosphere from the Pioneer Venus Sounder Probe (solid) and the VEGA 2 Lander ( ) (from Seiff et al 1987)

Figure 3. The zonally-averaged temperature field as a function of latitude from PV OIR observations. The dashed line shows the level of cloud optical depth unity (from Taylor et al. 1980).

Figure 4. Synthetic spectra of the thermal flux emitted by the Venus atmosphere for (i) nominal gas (30ppmv H_2O) and aerosol optical properties, (ii) nominal gas) optical properties, with aerosol absorption but no aerosol scattering, and (iii) nominal aerosol optical properties, but H_2O abundances from Venera 11/12 Spectrophotometer results (20–200ppmv).

Figure 5. Radiative cooling rates for (i) nominal gas (30ppmv H_2O) and aerosol optical properties, (ii) nominal gas) optical properties with aerosol absorption, but no aerosol scattering, and (iii) nominal aerosol optical properties, but H_2O abundances from Venera 11/12 Spectrophotometer results (20–200ppmv).

Figure 6. Solar heating rates and thermal cooling rates: (i) nominal gas and aerosol optical properties, (ii) 50% reductions in the middle and lower cloud aerosol optical depths, (iii) 60% increase in the middle and lower cloud aerosol optical depths: (a) globally-averaged solar heating rates, (b) heating rate differences, (c) thermal cooling.

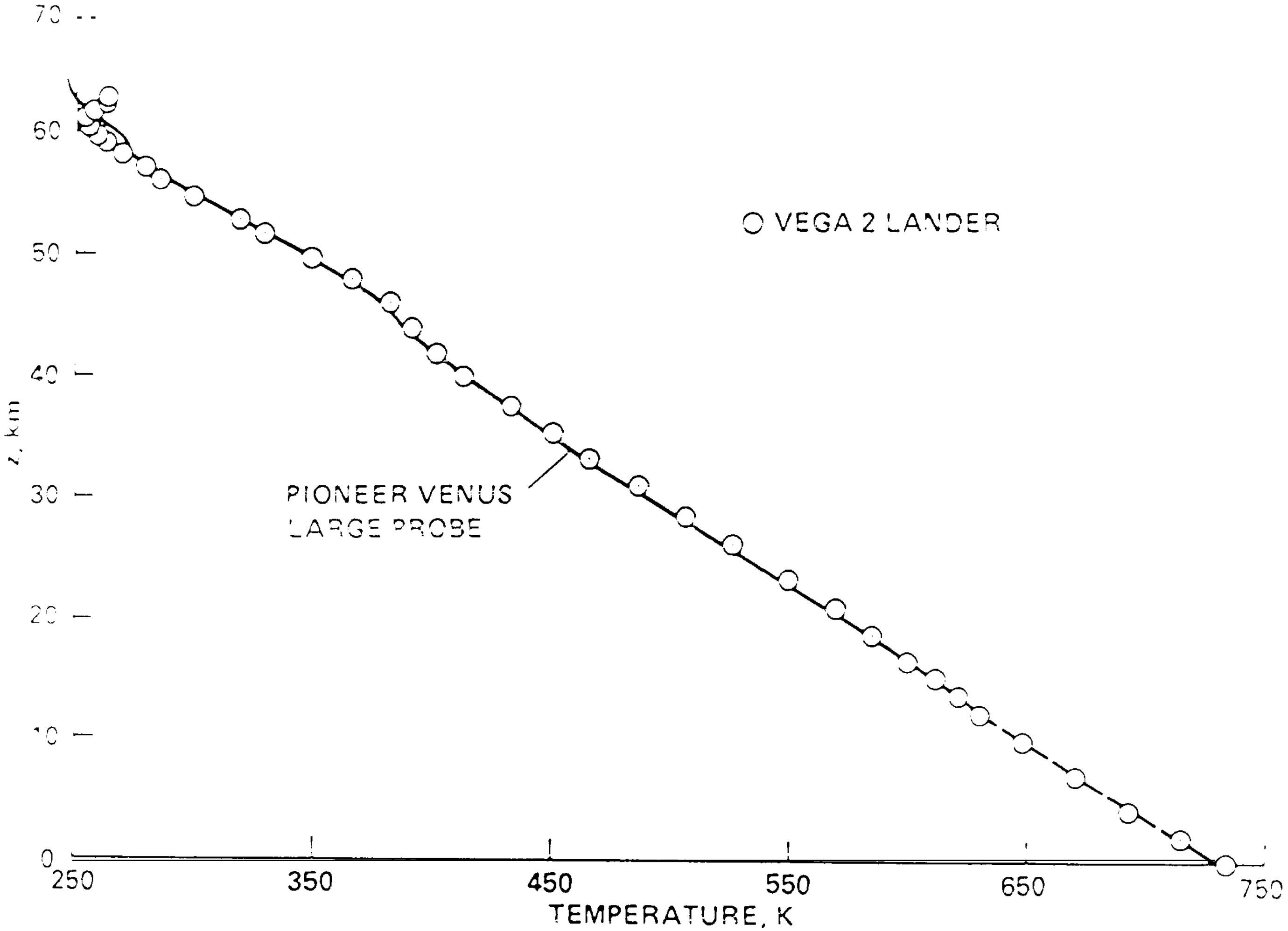
70
60
50
40
30
20
10
0
z, km
O VEGA 2 LANDER
PIONEER VENUS
LARGE PROBE
250
350
450
550
650
750
TEMPERATURE, K

FIG. 1

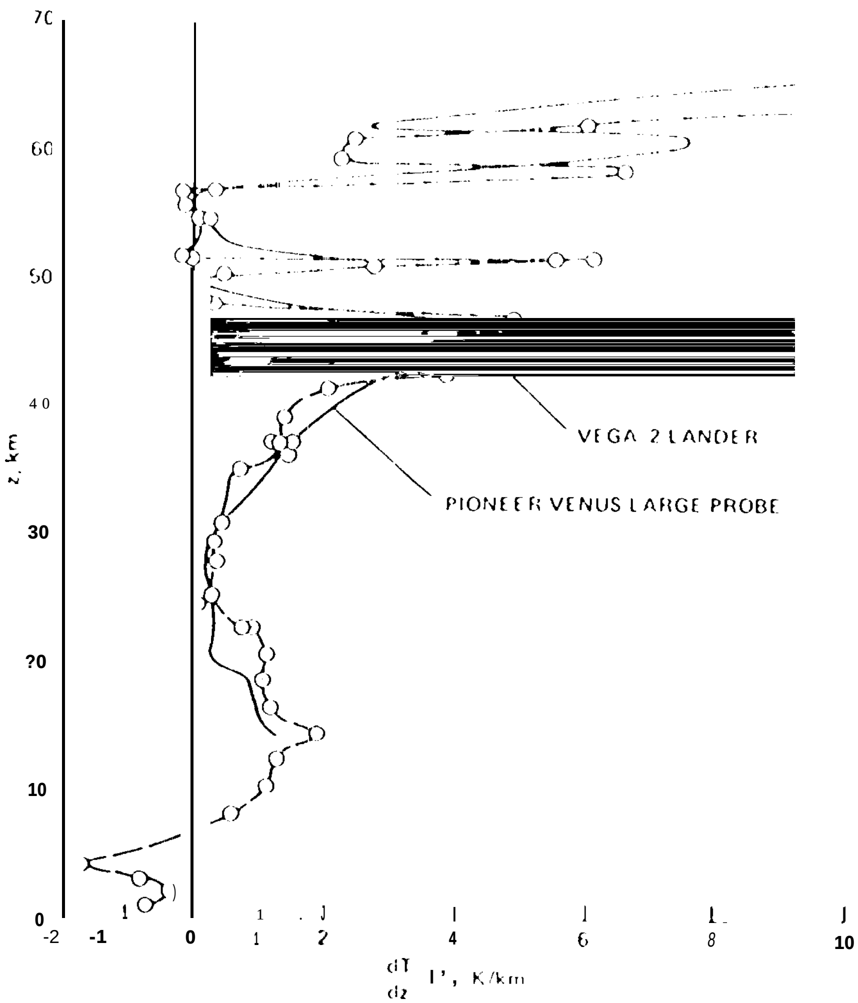
VEGA 2 LANDER
PIONEER VENUS LARGE PROBE
z, km
70
60
50
40
30
20
10
0
-2
-1
0
1
2
4
6
8
10
dT
dz
K/km

FIG. 2.

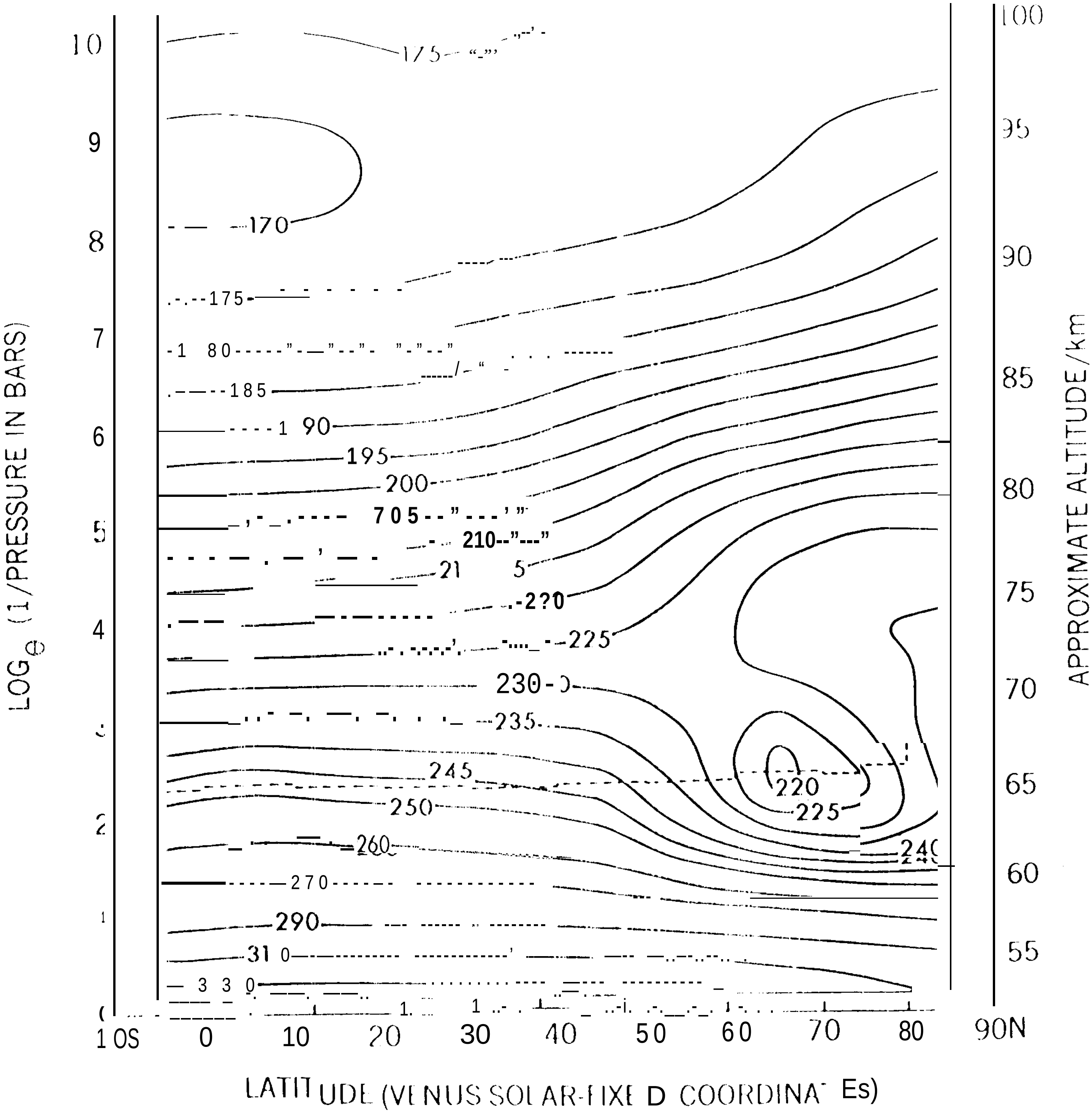

LOG_e (1/PRESSURE IN BARS)
APPROXIMATE ALTITUDE/km
LATITUDE (VENUS SOLAR-FIXED COORDINATES)
10
9
8
7
6
5
4
2
1
100
90
85
80
75
70
65
60
55
170
175
185
195
200
210
225
230
235
245
250
220
225
290
270
0
10
20
30
40
50
60
70
80
90N

FIG. 3

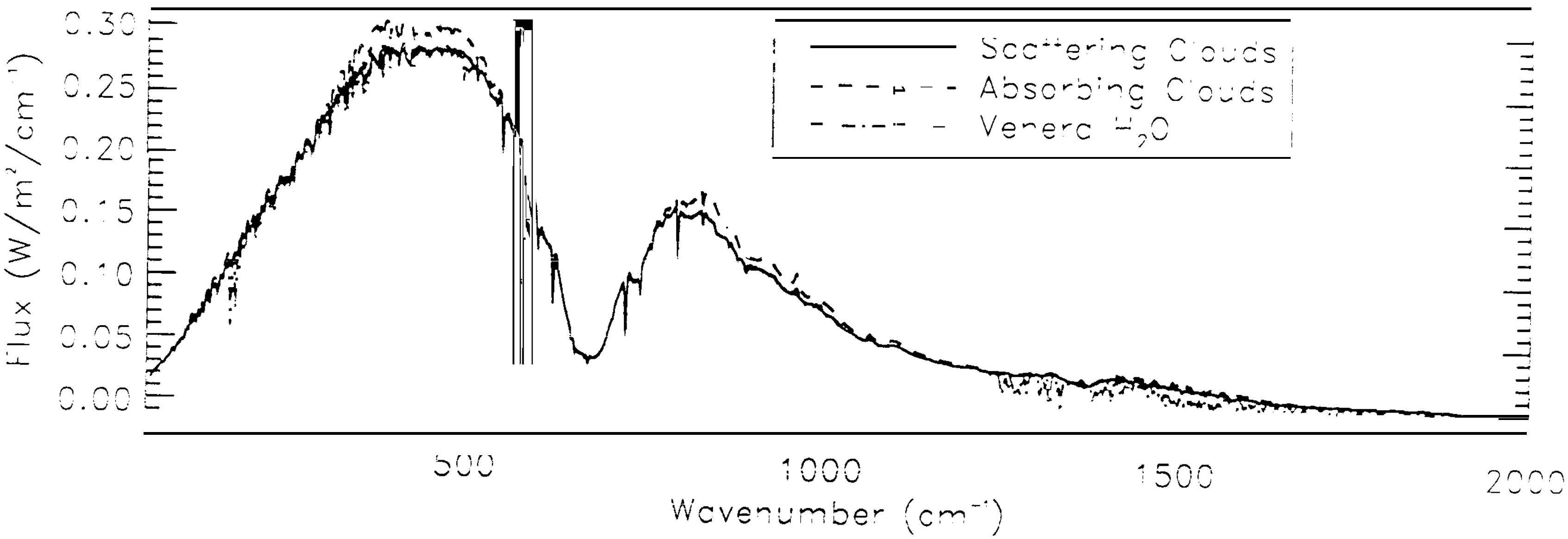
Scattering Clouds
Absorbing Clouds
Venera H_2O
Flux (W/m²/cm⁻¹)
0.00
0.05
0.10
0.15
0.20
0.25
0.30
500
1000
1500
2000
Wavenumber (cm⁻¹)

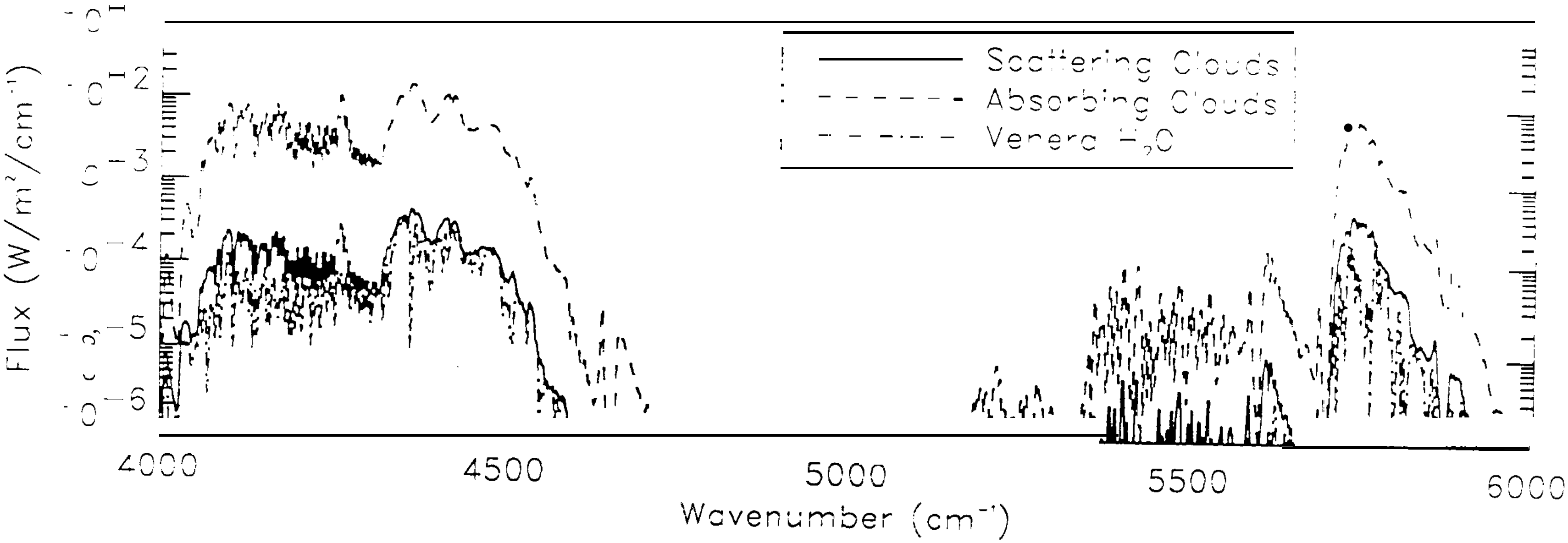
Scattering Clouds
Absorbing Clouds
Venera H_2O
Flux (W/m²/cm⁻¹)
4000
4500
5000
5500
6000
Wavenumber (cm⁻¹)

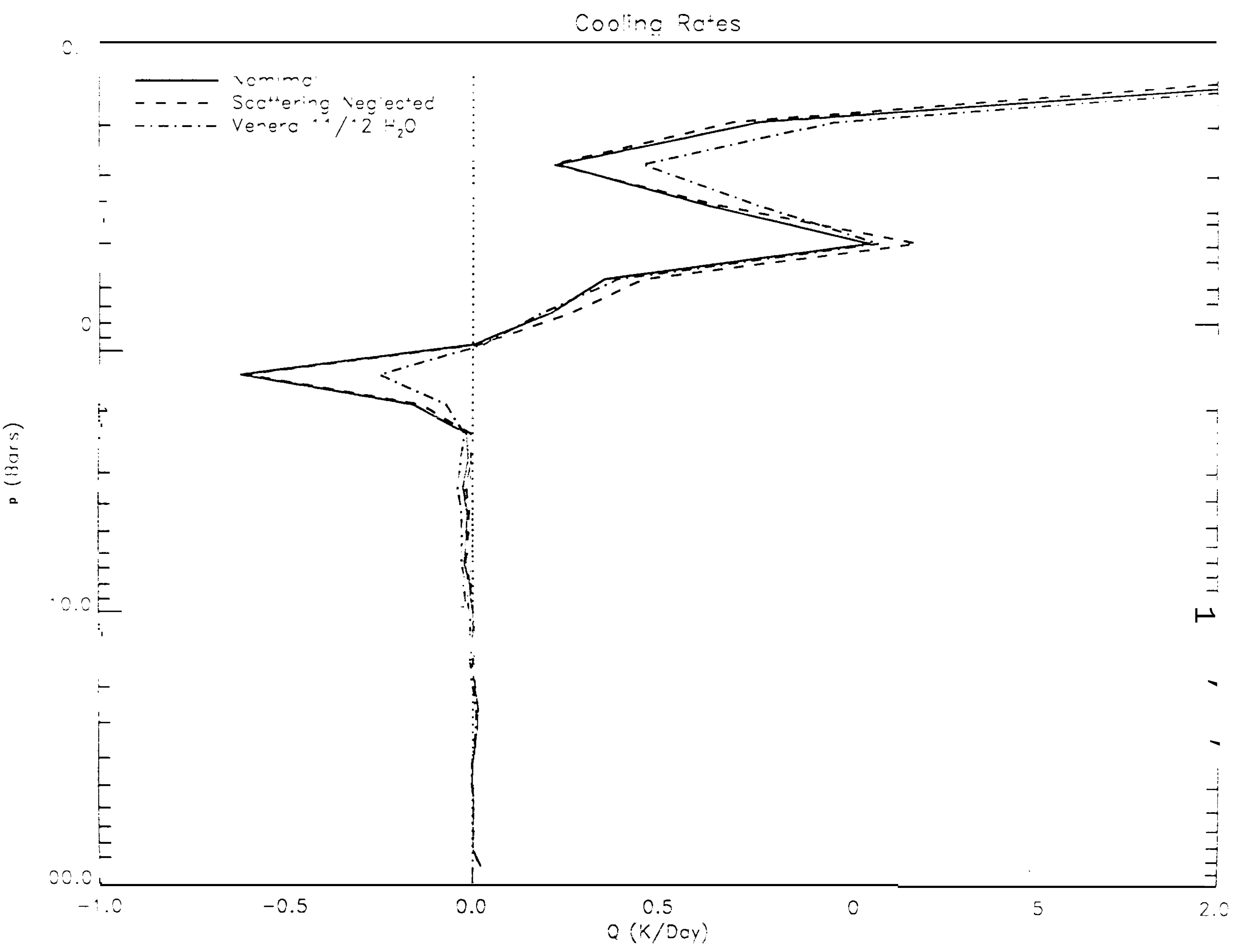
Cooling Rates
Nominal
Scattering Neglected
Venera 11/12 H_2O
p (Bars)
Q (K/Day)
-1.0
-0.5
0.0
0.5
2.0
10.0

F

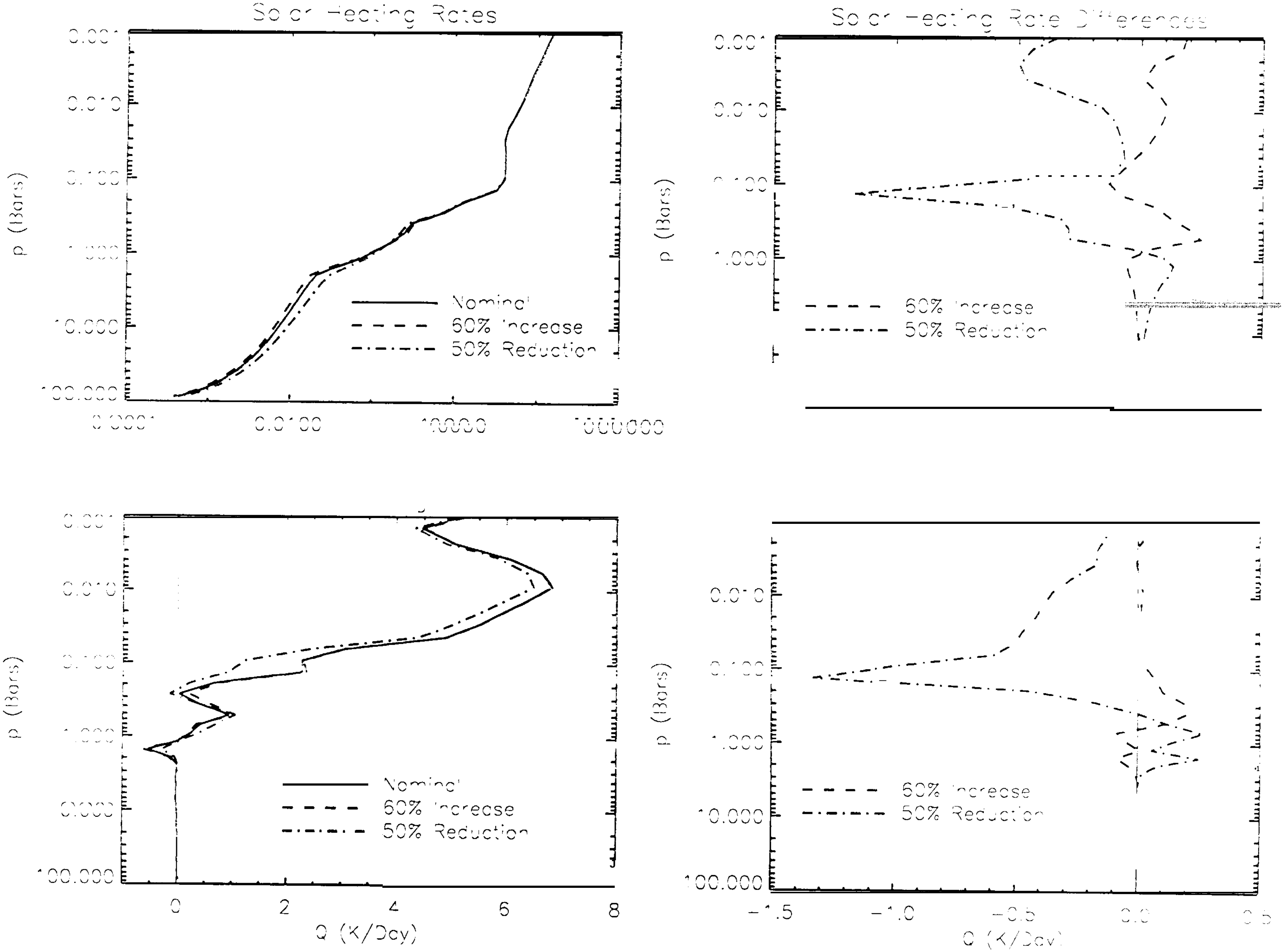

Solar Heating Rates
Solar Heating Rate Differences
p (Bars)
Nominal
60% Increase
50% Reduction
Q (K/Day)

FIG. 6

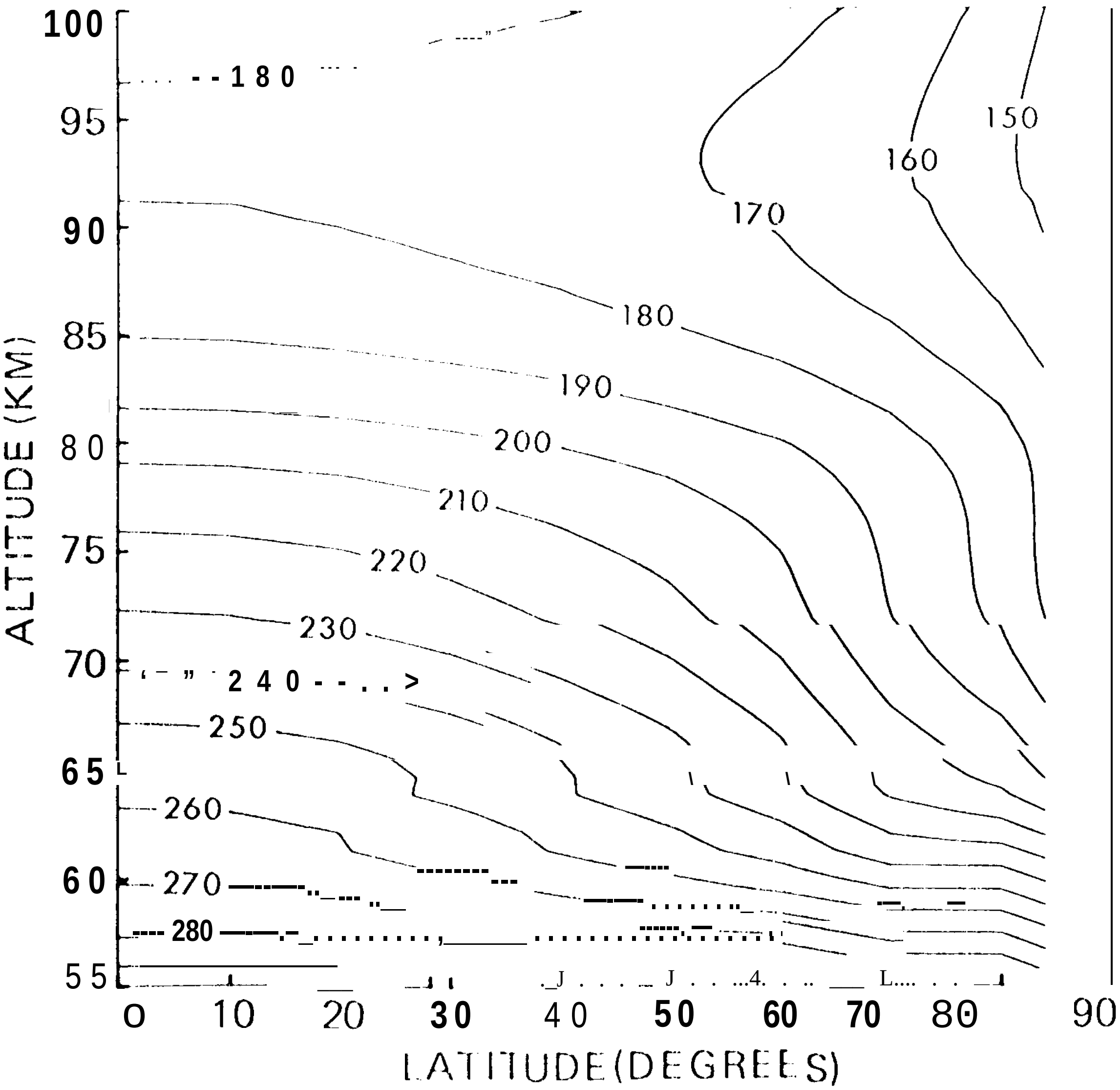
ALTITUDE (KM)
100
95
90
85
80
75
70
65
60
55
0
10
20
30
40
50
60
70
80
90
LATITUDE (DEGREES)
180
170
160
150
190
200
210
220
230
240
250
260
270
280

FIG. 7

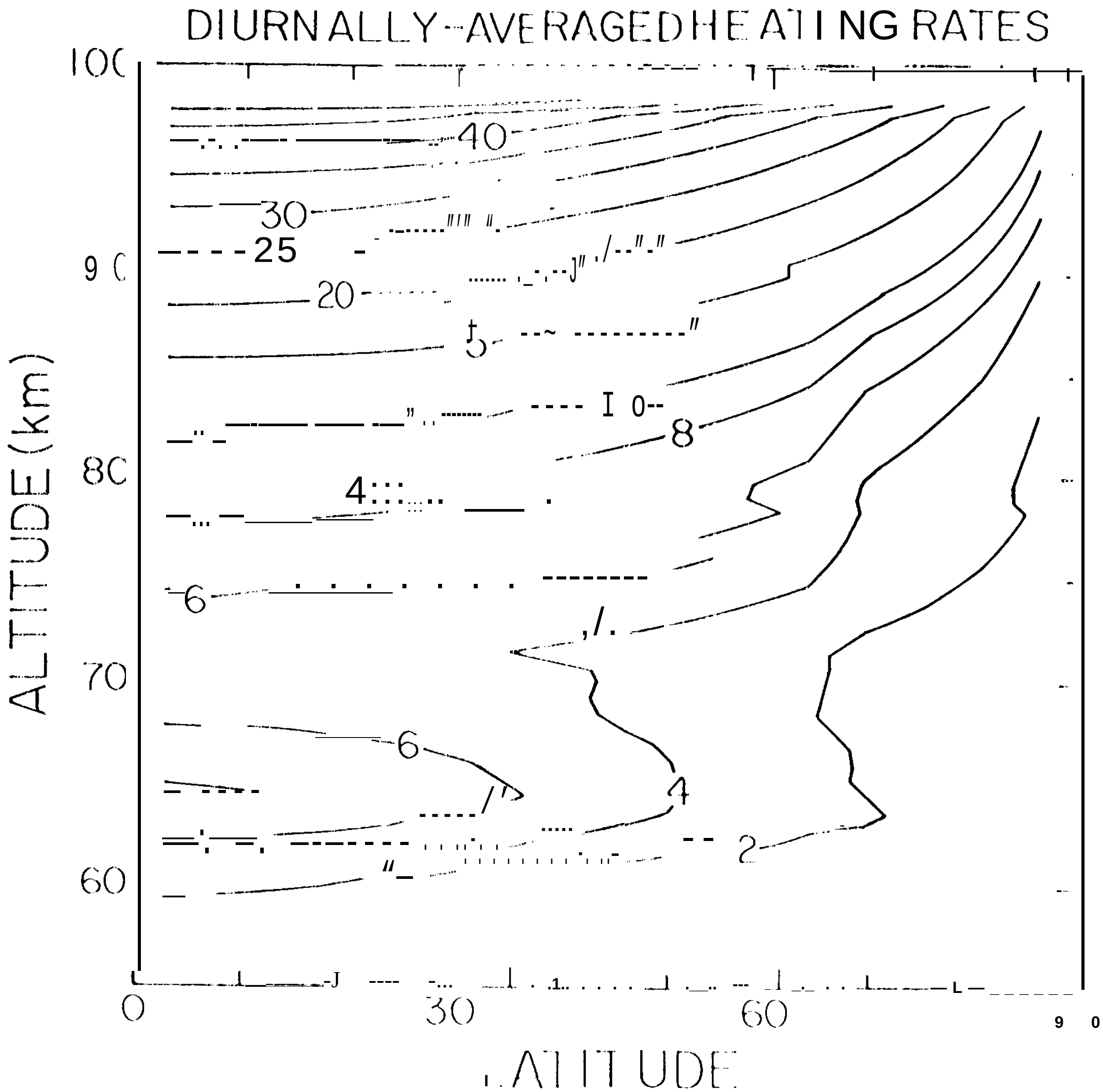
DIURNALLY-AVERAGED HEATING RATES
ALTITUDE (km)
LATITUDE
100
90
80
70
60
0
30
60
90
40
30
25
20
8
4
6
2

FIG. 8

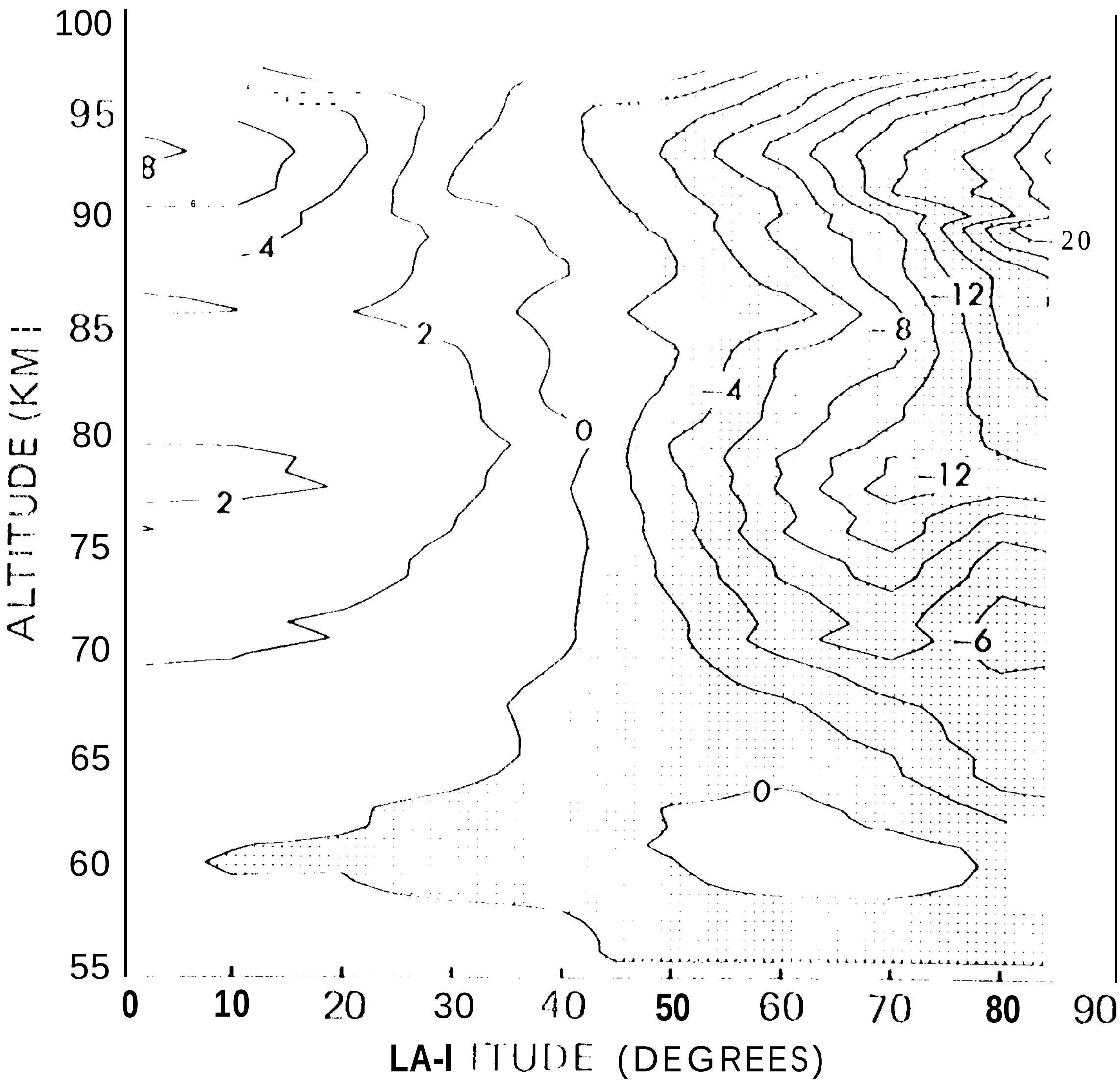

100
95
90
85
80
75
70
65
60
55
ALTITUDE (KM)
0
10
20
30
40
50
60
70
80
90
LATITUDE (DEGREES)
8
4
2
0
2
-4
-8
-12
-12
-6
0
20

FIG. 9

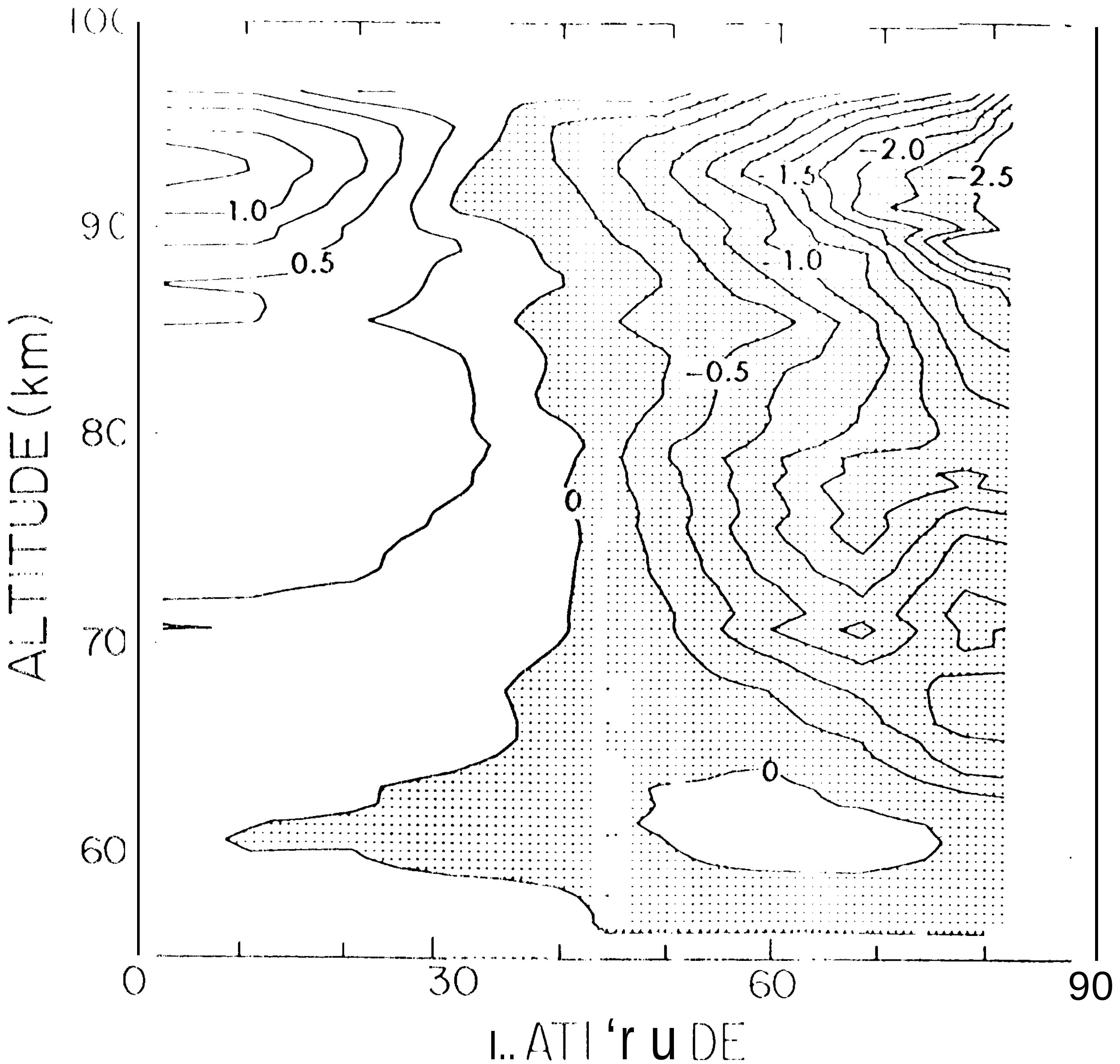

100
90
80
70
60
ALTITUDE (km)
0
30
60
90
LATITUDE
1.0
0.5
0
-0.5
-1.0
-1.5
-2.0
-2.5

FIG. 10